Forestry An International Journal of Forest Research

Institute of Chartered Foresters

Forestry 2021; **94**, 565–575, https://doi.org/10.1093/forestry/cpab023
Advance Access publication 10 May 2021

Biomass estimates derived from sector subsampling of 360° spherical images

Xiao Dai[1], Mark J. Ducey[2], Haozhou Wang[1], Ting-Ru Yang[1], Yung-Han Hsu[1], Jae Ogilvie[1] and John A. Kershaw Jr[1]

[1]*Faculty of Forestry and Environmental Management, University of New Brunswick, Fredericton, NB, Canada*
[2]*Department of Natural Resources and the Environment University of New Hampshire, Durham, NH, USA*

*Corresponding author: Tel: +1(506)453-4933; E-mail: xdai1@unb.ca

Received 28 January 2021

Efficient subsampling designs reduce forest inventory costs by focusing sampling efforts on more variable forest attributes. Sector subsampling is an efficient and accurate alternative to big basal area factor (big BAF) sampling to estimate the mean basal area to biomass ratio. In this study, we apply sector subsampling of spherical images to estimate aboveground biomass and compare our image-based estimates with field data collected from three early spacing trials on western Newfoundland Island in eastern Canada. The results show that sector subsampling of spherical images produced increased sampling errors of 0.3–3.4 per cent with only about 60 trees measured across 30 spherical images compared with about 4000 trees measured in the field. Photo-derived basal area was underestimated because of occluded trees; however, we implemented an additional level of subsampling, collecting field-based basal area counts, to correct for bias due to occluded trees. We applied Bruce's formula for standard error estimation to our three-level hierarchical subsampling scheme and showed that Bruce's formula is generalizable to any dimension of hierarchical subsampling. Spherical images are easily and quickly captured in the field using a consumer-grade 360° camera and sector subsampling, including all individual tree measurements, were obtained using a custom-developed python software package. The system is an efficient and accurate photo-based alternative to field-based big BAF subsampling.

Introduction

Aboveground biomass (AGB) plays a vital role in global climate change mitigation and ecosystem dynamics (Brown, 1997; Mette *et al.*, 2002; Le Toan *et al.*, 2011) and can help in monitoring emissions of CO_2 resulting from land use and land cover changes (Sales *et al.*, 2007). To restore, enhance and manage forest resources and create a sustainable environment (Bartuska, 2006), forest attributes must be efficiently monitored (Brown, 1999; Pearson *et al.*, 2007; Chen *et al.*, 2019). Direct measurement of biomass requires complete harvest of sample plots and drying and weighing of the different tree components (Kershaw *et al.*, 2016, pp. 153–154). This process is destructive, time-consuming and costly and is generally limited to a few research studies rather than used operationally. Accurate and repeatable estimates often are obtained from allometric equations applied to individual tree measurements (e.g. diameter at breast height (DBH) and height (HT)) and expanded to per unit area (Brown, 2002; Lu *et al.*, 2016); however, even this process is time-consuming and may result in large errors because relationships between species, forest ages, site conditions and equations must be considered (Telenius and Verwijst, 1995; Lu, 2006; Yang *et al.*, 2017). Various indirect methods such as regression models (Baskerville, 1972; Brown *et al.*, 1989; Usoltsev and Hoffmann, 1997; Montès *et al.*, 2000), hemispherical photography (Clark and Murphy, 2011) and remote sensing (Armstrong, 1993; Lu, 2006; Zolkos *et al.*, 2013; Lu *et al.*, 2016) are used for AGB estimation. However, there is no standard for determining the best estimation methods for biomass because various data sources and prediction approaches are frequently applied (Fassnacht *et al.*, 2014), even though they can give widely varying results (e.g. MacLean *et al.*, 2014). The most effective variables, equation forms and estimation approaches are not clear (Lu *et al.*, 2016) and have not, to our knowledge, been systematically studied.

Remote sensing is an important tool for landscape level biomass estimation (Lu, 2006). Light Detection and Ranging (LiDAR), either airborne (ALS) or terrestrial (TLS), scanning has shown promise for biomass estimation (Goetz *et al.*, 2009; Gleason and Im, 2011; Hayashi *et al.*, 2015) and has become an almost ubiquitous tool in forest inventory (Dubayah and Drake, 2000; Dassot *et al.*, 2011; Hayashi *et al.*, 2015). ALS has the capability of covering large landscapes and providing high-resolution ground and canopy surface models (Gaveau and Hill, 2003; Räsänen *et al.*, 2014; Wilkes *et al.*, 2015; Erfanifard *et al.*, 2018), while TLS has the capability of estimating understory vegetation parameters (Hilker *et al.*, 2010; Hopkinson *et al.*, 2013), calibrating ALS estimates with auxiliary variables (Greaves *et al.*, 2017) and providing forest structural information (Ducey and Astrup, 2013; Astrup *et al.*, 2014). However, LiDAR is not without its shortcomings. Occlusion of all or parts of some trees is a frequent issue with both ALS and TLS (Hilker *et al.,* 2010; Ducey and Astrup, 2013; White *et al.,* 2016) and is a major source of uncertainty in LiDAR-assisted forest inventories (Ayrey *et al.,* 2019). Reliance on model-assisted predictions based on data that are not probabilistic samples is another source of uncertainty (Yang *et al.,* 2019). While ALS data are becoming increasingly freely available, terrestrial scanners remain very expensive and both data sources require field data for calibration, extensive postprocessing, model fitting and prediction verification. In many respects, LiDAR trades off costs associated with field work with costs associated with equipment and office work.

Close-range digital photogrammetry is a cost-effective alternative to TLS (Stewart *et al.,* 2004; Perng *et al.,* 2018; Lu *et al.,* 2019; Wang, 2019). Several researchers have demonstrated that high-resolution panoramic imagery is an accurate tool for collecting basic tree and forest data (Dick *et al.,* 2010; Fastie, 2010; Lu *et al.,* 2019;Wang, 2019 ; Wang *et al.,* 2020). Horizontal point sampling (or angle count sampling (Bitterlich, 1984; Iles, 2003; Stewart *et al.,* 2004)) is easily implemented on 360° panoramic images (Fastie, 2010; Dick, 2012). The angle required for a given basal area factor is expressed in terms of pixels, and a pixel-based 'gauge' is moved across the image, and trees appearing larger than the gauge are counted as 'in' trees (DeCourt, 1956; Stewart *et al.,* 2004; Fastie, 2010; Dick, 2012; Wang *et al.,* 2020). However, occluded (hidden or partially hidden by closer trees) trees are a problem with photo-based angle count sampling resulting in undercounts of 'in' trees and, as a result, photo basal area (PBA) is underestimated (Stewart *et al.,* 2004; Dick, 2012; Wang, 2019). In addition to PBA estimates, Perng *et al.* (2018) and Lu *et al.* (2019) demonstrated how individual tree diameters and heights can be obtained from stereographic 360°/180° hemispherical images, and Wang *et al.* (2021) extended this idea to spherical images.

The newer consumer-grade 360° spherical cameras make photo-based angle count sampling even easier because image stitching is done onboard the camera and the two fixed fish-eye lenses minimize alignment errors (Wang, 2019; Wang *et al.,* 2020). Dai (2021) compared biomass estimation models based on PBA derived from spherical images obtained using a Ricoh Theta S 360° camera (Ricoh Imaging Company, LTD, 2016) to models based on common TLS metrics. Root mean square errors (rMSEs) for models based on TLS metrics ranged from 20 to 33 per cent, while rMSEs for models derived from PBA estimates ranged from 17 to 21 per cent. Given the low cost, portable size and field efficiency, the spherical camera offers much promise as a forest inventory tool (Wang *et al.,* 2020; Dai *et al.* 2021, in press).

Model development requires calibration for every new application. Efficient sample-derived estimation may be an effective alternative to model estimates (Yang *et al.,* 2019). Big basal area factor (BAF) sampling is a widely used subsampling design that utilizes a small angle gauge to count 'in' trees and estimate basal area per ha (BA; $m^2 ha^{-1}$) for each sample point; and a larger angle gauge to select trees to measure (Iles, 2003; Marshall *et al.,* 2004; Yang *et al.,* 2017). The ratio of the tree attribute of interest to individual tree BA (XBAR) calculated from the measure-trees and the mean BA are used to calculate the per unit area estimates of the attribute of interest. However, implementing big BAF sampling on spherical photos is challenging, since big BAF sampling tends to select trees that are very close to the sample point. On spherical images, these trees are often very distorted, or it is very difficult to clearly identify the tree tip which make tree height harder to measure accurately (Wang *et al.,* 2021). An effective subsampling protocol for spherical image sampling requires an alternative measure-tree selection process.

Dai *et al.* (2021, in press) showed that sector subsampling is a viable alternative measure-tree selection method to big BAF sampling with differences in mean values averaging less than 1 per cent of the means obtaining using big BAF sampling and nearly equivalent standard errors for a given measure-tree subsample intensity (i.e. number of trees). Sector sampling (Iles and Smith, 2006; Smith *et al.,* 2008; Smith and Iles, 2012) uses sectors of a circle to define sample plots. Originally designed to efficiently sample small or irregular forest areas (Iles and Smith, 2006; Smith *et al.,* 2008; Smith and Iles, 2012), Dai *et al.* (2021, in press) applied sectors as a means to select subsamples of trees for detailed measurement. As formulated by Dai *et al.* (2021, in press), sector subsampling uses a small angle gauge and horizontal point sampling to select count trees to estimate BA and then a randomly oriented sector to select a subsample of trees to measure. Two variants of sector subsampling were developed. The first method, termed SectorIN, used a randomly oriented sector to select a subsample of the 'in' trees selected using the small angle gauge. All 'in' trees that fell within the sector were selected as measure trees. The second method, termed SectorDST, used a randomly oriented sector to select a subsample trees within a predefined distance of plot centre for measurement. In this case, measure-trees could be either 'in' trees or other trees that fell within the predefined sector. Like big BAF sampling, the measure trees are used to estimate the ratio of the tree attribute of interest to tree basal area, and the mean ratio is multiplied by average BA to estimate the per ha average of the attribute of interest.

In this paper, we combine photo point sampling (Stewart *et al.,* 2004; Fastie, 2010; Dick, 2012; Wang *et al.,* 2020) with sector subsampling (Dai *et al.* 2021, in press) to develop an efficient method for sample-derived estimation of area-based AGB using spherical images. The specific objectives of this study were: (1) apply sector subsample selection to PBA plots obtained from spherical images; (2) develop a hierarchical approach to subsampling from photos that includes correction for occluded trees and (3) generalize Bruce's formula (Goodman, 1960) for multiple subsample levels.

Methods

Study sites

In this study, data from western Newfoundland Island (NL), Canada, were used. These data came from three early spacing trials established in the early 1980s by the government of Newfoundland and Labrador in cooperation with the Canadian Forest Service (Donnelly *et al.,* 1986) (Figure 1). Balsam fir (*Abies balsamea* L.) was the dominant species with minor components of black spruce (*Picea mariana* (Mill.) Britton, Sterns and Poggenb.) and white birch (*Betula papyrifera* Marshall). There were five spacing treatments: control/no spacing (S00), 1.2-m spacing (S12), 1.8-m spacing (S18), 2.4-m spacing (S24) and 3.0-m spacing

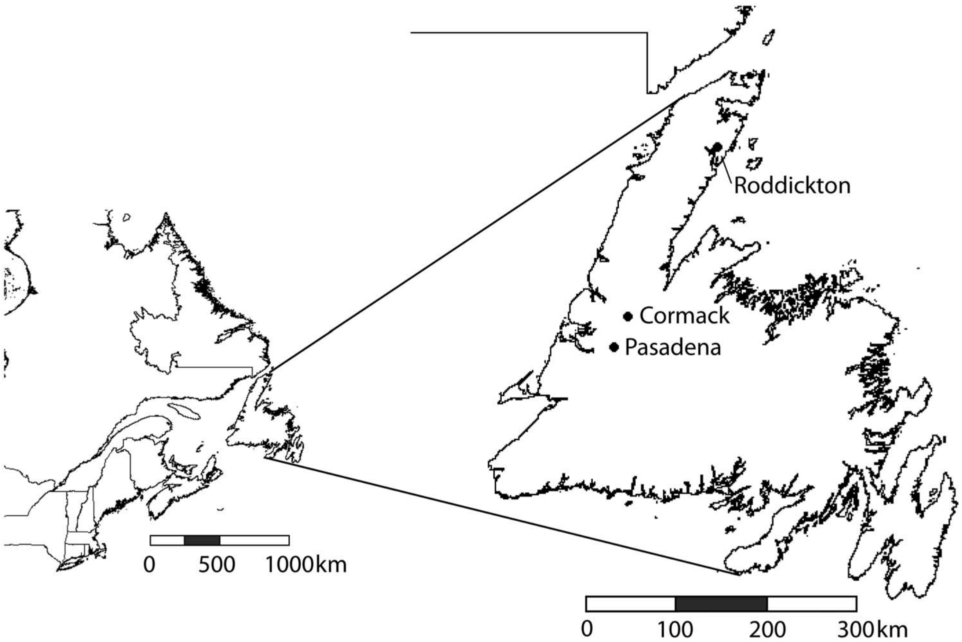

Figure 1 Location of Newfoundland in Atlantic Canada and locations of three early spacing trials on Newfoundland Island.

(S30). The treatments were arranged in a randomized complete block design with 3 blocks per trial (45 sample units were used in this study). Each treatment was applied to a 0.25-ha area (50 m × 50 m), and a circular permanent sample plot (PSP) was established near the centre of each 0.25-ha area. The PSP size varied such that there were ~100 trees per plot at the time of establishment. Only the most recent measurements for each trial were used in this study (2013 for Pasadena and Cormack; 2017 for Roddickton).

Field biomass estimation

Individual tree biomass was estimated using the Canadian National Biomass equations (Lambert *et al.,* 2005). We used Eq. 3 from Table 4 in Lambert *et al.* (2005) which included both DBH (cm (BH = 1.3 m above ground)) and total height (HT; m). Total tree biomass (BM_i; kg) was obtained by summing the separate component biomass estimates (wood, bark, branches and foliage). Field biomass per ha (FBM; tonnes·ha^{-1}) for each sample point was estimated by summing the individual tree biomass estimates multiplied by the plot expansion factor and dividing by 1000 kg per tonne

$$\mathrm{FBM} = \frac{EF \times \sum_{i=1}^{n} \mathrm{BM_i}}{1000}, \tag{1}$$

where n = the number of field measure trees on each PSP.

Sector subsampling of spherical images

A Ricoh Theta S 360° camera (Ricoh Imaging Company, LTD, 2016) was used to obtain spherical images of the NL spacing trial PSPs. We obtained images in three locations on each PSP. The images were obtained at half the plot radius of each PSP at azimuths of 0° (360°), 120° and 240°. At each image acquisition location, spherical images were obtained at heights of 1.6 and 2.6 m using a tripod-stabilized height pole (Wang *et al.,* 2021).

In Dai *et al.* (2021, in press), sector subsampling intensity was defined in terms of the angular percentage of the 360° azimuth subsampled (Figure 2a). The software developed by Wang *et al.* (2021) was modified to randomly select a sector of a specified intensity by randomly generating an azimuth and superimposing parallel vertical lines on the cylindrically projected images based on sector intensity (Figure 2b) with the inclusion region centred on the randomly generated azimuth (in cylindrical projections, fixed horizontal angles are of fixed image width; thus the vertical parallel lines project the specified sector angle onto the cylindrical image; Figure 2b).

In our first simulation experiment, a modified SectorDST sampling method (Dai *et al.* 2021, in press) was implemented on each photo pair at each image acquisition location within each PSP (three locations per PSP were used in this study) across the three spacing trials to select measure-trees to determine the mean biomass to basal area ratio ($\overline{\mathrm{BBAR}}$; kg·m^2). PBA (m^{2}ha^{-1}) was estimated from the spherical images (1.6-m image heights) using the software (available from: https://github.com/HowcanoeWang/Panorama2BasalArea) developed by Wang *et al.* (2020) and a 2 M BAF (i.e. each count tree represents 2 m^{2}ha^{-1} of basal area). Mean PBA for each PSP was estimated using

$$\overline{\mathrm{PBA}} = \frac{\sum_{i=1}^{p} \mathrm{PBA_i}}{p} = \frac{\sum_{i=1}^{p} \mathrm{BAF} \times \mathrm{Count_i}}{p}, \tag{2}$$

where p = the number of image acquisition locations (three in the study).

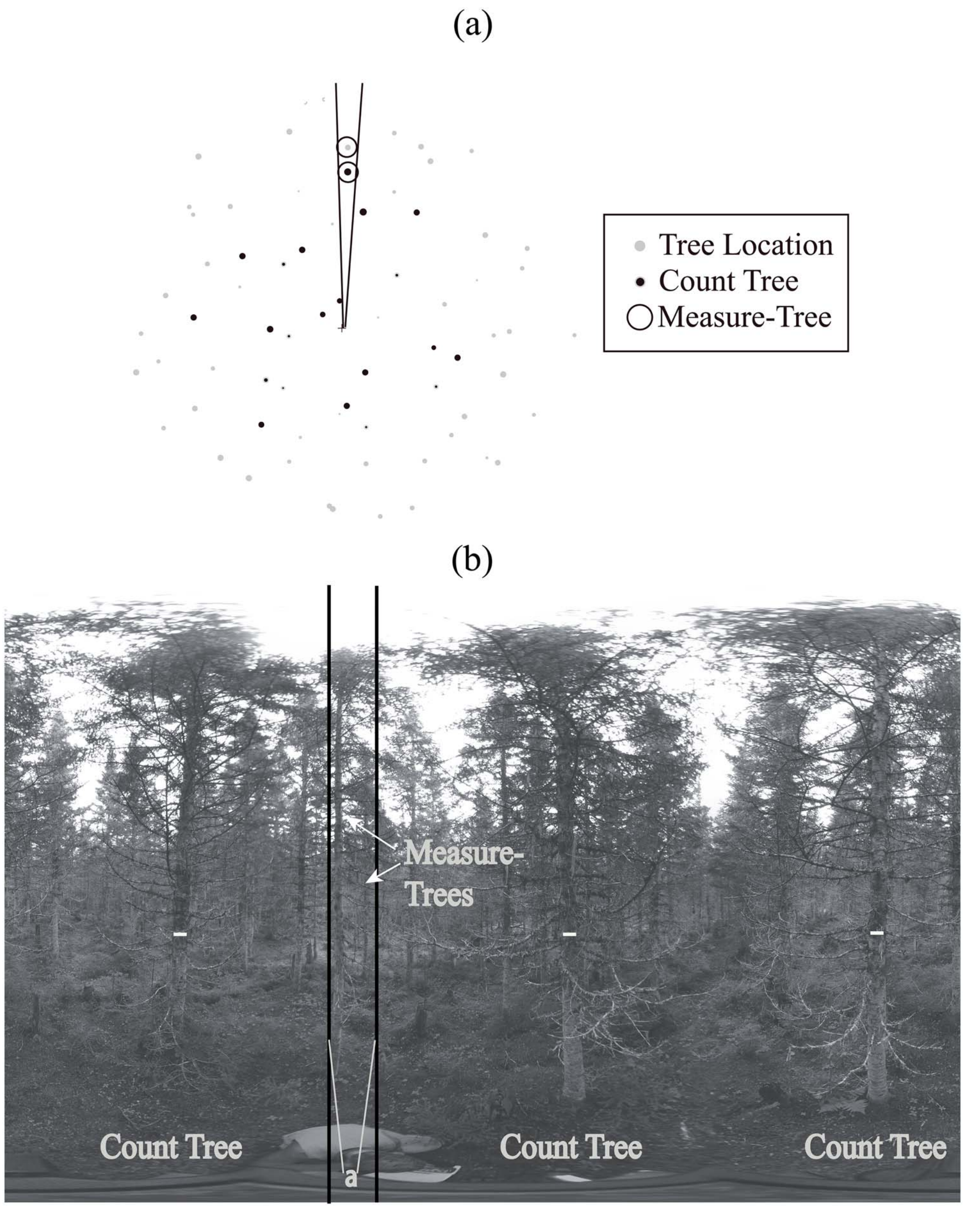

Figure 2 SectorDST subsampling as viewed: (a) from a map perspective of a photo sample plot and (b) as viewed from a cylindrically projected spherical image. (BAF count trees are identified by horizontal white bars; measure trees are those trees within the two vertical black lines defined by sector angle 'a').

The SectorDST selection method, as developed in Dai *et al.* (2021, in press), selects measure-trees within a randomly oriented sector within a predetermined distance from the sample point (Figure 2a). For the spherical images, tree occlusion is an issue, so instead of selecting all trees within a given distance, we chose all trees within a sector that were clearly visible (Figure 2b). All visible trees within the sector were measured for DBH (PDBH) and HT (PHT) on the spherical image pairs using the stereographic methods described by Wang *et al.* (2021) as implemented in the modified software (available from: https://github.com/HowcanoeWang/Spherical2TreeAttributes).

Photo tree basal area (PTBA) and photo tree biomass (PTBM) were calculated using the same methods described above for the field estimates (assuming all trees were balsam fir for biomass estimation) and mean BBAR ($\overline{\text{BBAR}}$) was calculated using a ratio of means approach (Dai *et al.* 2021, in press)

$$\overline{\text{BBAR}} = \frac{\sum_{i=1}^{m} \text{PTBM}_i}{\sum_{i=1}^{m} \text{PTBA}_i} = \frac{\sum_{i=1}^{m} \text{PTBM}_i}{\sum_{i=1}^{m} 0.00007854 \times (\text{PDBH}_i)^2}, \quad (3)$$

where m = the number of measure-trees. Mean photo biomass per ha (PBM, tonnes·ha^{-1}) was then estimated using

$$\overline{\mathrm{PBM}} = \frac{\overline{\mathrm{BBAR}} \times \overline{\mathrm{PBA}}}{1000}. \tag{4}$$

Percent standard error for (PBM) was estimated using Bruce's formula (Goodman, 1960; Marshall *et al.,* 2004)

$$\%\mathrm{se}\left(\overline{\mathrm{PBM}}\right) = \sqrt{\%\mathrm{se}\left(\overline{\mathrm{PBA}}\right)^2 + \%\mathrm{se}\left(\overline{\mathrm{BBAR}}\right)^2}, \tag{5}$$

where %se() = the standard error as a percent of the mean. Although Bruce's formula assumes independence of the error components, simulations show that it performs well in comparison with more complicated formulations (Gove *et al.,* 2020). For $\%\mathrm{se}\left(\overline{\mathrm{PBA}}\right)$, we used the formula for standard error (se) under simple random sampling (Zar, 1999)

$$\mathrm{se} = \sqrt{\frac{\sum \mathrm{PBA}^2 - \left(\sum \mathrm{PBA}\right)^2/k}{k\,(k-1)}}, \tag{6}$$

where k = the number of sample plots. For $\%\mathrm{se}\left(\overline{\mathrm{BBAR}}\right)$, we used the formulation provided in Kershaw *et al.* (2016 p. 348, Eq. 10.53)

$$\%\mathrm{se}\left(\overline{\mathrm{BBAR}}\right) = \sqrt{\left(\frac{\overline{\mathrm{BBAR}}^2}{m\,(m-1)}\right)\left(\frac{\sum \mathrm{PTBM}^2}{\overline{\mathrm{PTBM}}^2} + \frac{\sum \mathrm{PTBA}^2}{\overline{\mathrm{PTBA}}^2} - \frac{2\sum \mathrm{PTBM}\cdot\mathrm{PTBA}}{\overline{\mathrm{PTBM}}\cdot\overline{\mathrm{PTBA}}}\right)}, \tag{7}$$

where PTBM and $\overline{\mathrm{PTBM}}$ were the individual measure-tree biomass estimates and mean measure-tree biomass estimates; PTBA and $\overline{\mathrm{PTBA}}$ were the individual measure-tree stem basal areas (estimated from PDBH measures triangulated from the 1.6- and 2.6-m images) and mean measure-tree stem basal area and $\overline{\mathrm{BBAR}}$ was the mean biomass to basal area ratio of the measure-trees from Eq. 3.

The SectorDST sampling procedure was implemented on each spherical image pair at each image acquisition point on each spacing PSP on each replicate across the three spacing trials (3 trials × 5 treatments × 3 blocks × 3 locations = 135 image acquisition points). All analyses were conducted in the R Statistical Language (R Development Core Team, 2019).

Occluded tree correction

One sampling issue with using PBA is tree occlusion (Dick, 2012). On photo plots, it is not possible to move from the sample point to check for occluded (hidden) trees. Occluded trees result in under–counting of 'in' trees and negative biases in BA estimates. To explore the potential of using a subsample of in-field tree counts to correct for PBA bias, we implemented a simulation study using the spherical image results from the previous section and a subsample of field basal area (FBA) counts. We explored field BA: PBA correction (field to photo basal area ratio, FPBAR) by randomly selecting 5, 10, 15 or 20 plots to obtain FBA measures. A second ratio of means estimator was obtained to correct PBA using the subsampled field BAs

$$\overline{\mathrm{FPBAR}} = \frac{\sum_{i=1}^{j} \mathrm{FBA}_i}{\sum_{i=1}^{j} \mathrm{PBA}_i}, \tag{8}$$

where $\overline{\mathrm{FPBAR}}$ was the mean of FBA to PBA ratio, j = the number of field plots used for correcting PBA (5, 10, 15, 20 in this study), and the corrected biomass estimate ($\overline{\mathrm{CBM}}$) became

$$\overline{\mathrm{CBM}} = \overline{\mathrm{FPBAR}}\cdot\overline{\mathrm{PBM}} = \overline{\mathrm{FPBAR}}\cdot\left(\overline{\mathrm{PBA}}\cdot\overline{\mathrm{BBAR}}\right). \tag{9}$$

We further used an extension of Bruce's formula to include this third source of sampling error

$$\%\mathrm{se}\left(\overline{\mathrm{CBM}}\right) = \sqrt{\%\mathrm{se}\left(\overline{\mathrm{FPBAR}}\right)^2 + \%\mathrm{se}\left(\overline{\mathrm{BBAR}}\right)^2 + \%\mathrm{se}\left(\overline{\mathrm{PBA}}\right)^2}, \tag{10}$$

where $\%\mathrm{se}\left(\overline{\mathrm{FPBAR}}\right)$ was estimated using Eq. 4. Derivation of Eq. 10 is given in the Supplemental Materials (Derivation of CBM Error). To assess the validity of this extension, we used coverage based on nominal 95 per cent confidence intervals and the correlations between the sources of errors. All simulations were repeated 100 times for estimation comparisons and 1000 times for assessing coverage of nominal confidence intervals.

Results

Using a sector intensity of 2 per cent (7.2° of the full 360°), 163 photo measure-trees were selected across the 135 image acquisition points (three points per PSP) over the 45 spacing trial PSPs. BBAR averaged 3214 kg·m^{-2} with a standard error of 30.7 kg·m^{-2}. PBA averaged 34.3 m^{2}ha^{-1} with a standard error of 1.8 m^{2}ha^{-1}. The resulting mean biomass was 110.3 kg·ha^{-1} with a standard error of 5.4 kg·ha^{-1} (Table 1). PBM was underestimated relative to FBM on all but two of the 45 spacing trial plots (Figure 3).

While underestimation of biomass was evident in the sector subsampling, the LOWESS smoothing line (Cleveland, 1981) indicated a relatively strong linear relationship that could be corrected using ratio estimation (Figure 3). Based on 100 repeated simulation samples using 1 image acquisition point per spacing PSP and a random subsample of FBA to correct PBA, the underestimation associated with PBA was efficiently corrected (Figure 3; Table 1). As few as 5 field plots were sufficient to correct the $\overline{\mathrm{PBM}}$ underestimation that resulted from occluded trees in the PBA estimates (Table 1). With 10 field samples, standard errors (Table 1) were comparable to those obtained using the regression estimates of $\overline{\mathrm{BM}}$ developed in Dai (2021, pp. 24 & 27), and with 20 subsamples, the standard errors were nearly

Table 1 Means and associated percent standard errors for biomass (tonnes·ha^{-1}) by study source (field measurements, terrestrial LiDAR scanning (TLS) and PBA regression-based predictions (Dai, 2021), and corrected/uncorrected sector subsampling estimates) and the associated corrected ratios by PBA correction subsample size for the western Newfoundland (NL) spacing trials. Ranges are shown in brackets {} (The correction ratios were determined by dividing FBA by PBA)

Source	Correction ratio		Biomass estimate	
Sample size	Mean[a]	Standard error (%)	Mean[b]	Standard error (%)
Field measured			148.9	7.3
TLS prediction			148.8	17.2
PBA prediction			149.3	19.9
Sector subsampling				
Uncorrected			102.9	5.4
5	1.44	20.1	148.5	30.1
	{0.93, 2.35}		{95.5, 241.7}	
10	1.42	13.4	146.4	19.7
	{1.03, 1.86}		{105.8, 191.4}	
15	1.40	9.3	144	13.2
	{1.06, 1.66}		{108.8, 171.2}	
20	1.40	7.1	143.9	10.3
	{1.18, 1.60}		{121.9, 163.5}	

[a]Correction ratio is unitless since it is field BA (m^{2}ha^{-1}) divided by photo BA (m^{2}ha^{-1}). [b]Biomass is in tonnes·ha^{-1}.

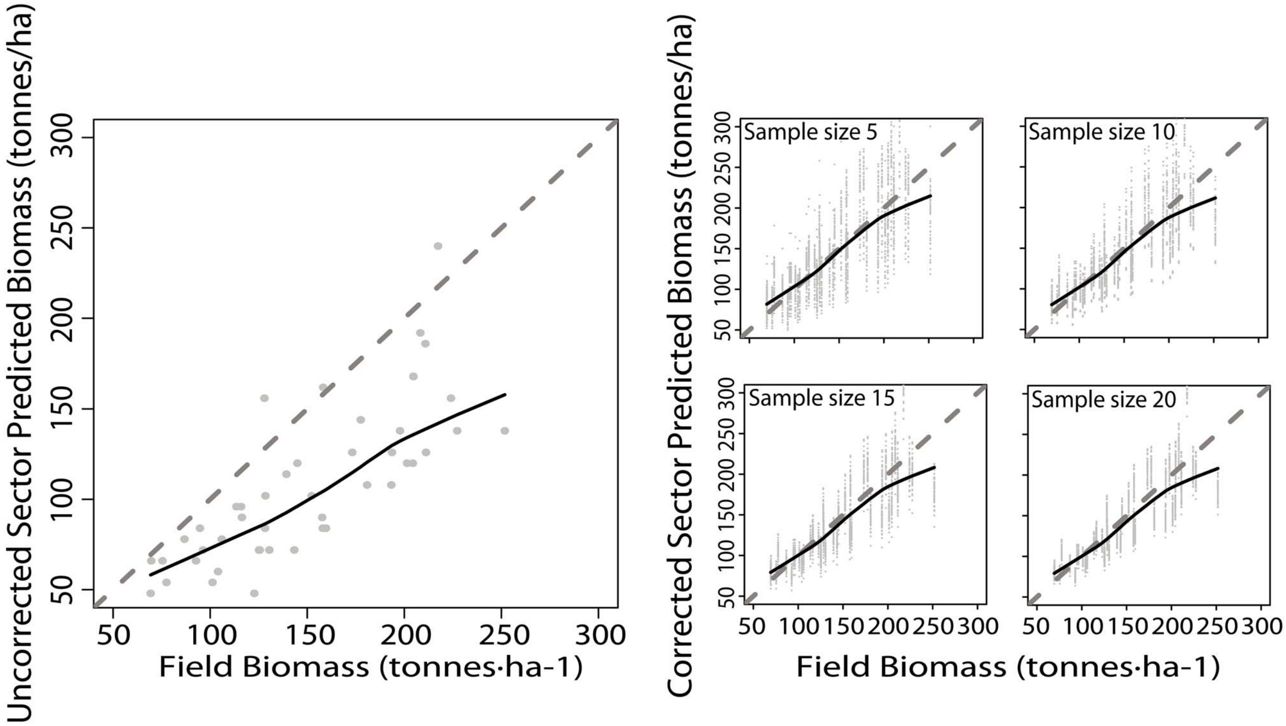

Figure 3 Corrected/uncorrected sector subsampled biomass estimates versus biomass estimated from field measurements under four different field BA correction sample sizes 5, 10, 15 and 20 for the Newfoundland (NL) spacing trials.

equivalent to those obtained for the complete field data from the 45 spacing plots with all trees measured for HT and DBH (Table 1). The 45 plots across the 3 spacing trials had 4181 trees measured with a standard error of 7.3 tonnes·ha^{-1}. In our simulations presented in Figure 3 and Table 1, there were, on average, 54 trees subsampled for photo measurement across the 45 randomly sampled spacing trial plots with an average standard error of 10.3 tonnes·ha^{-1}.

The addition of subsampling field PSPs for BA estimation and ratio correction added another source of error associated with our estimate of biomass. As expressed in Eq. 10, we proposed to expand Bruce's formula by adding a third component to the

Table 2 Comparison of percent standard errors from the sector-sample simulations for PBA ($m^2 ha^{-1}$), biomass to basal area ratio (BBAR; $kg{\cdot}m^{-2}$), field to photo BA ratio (FPBAR; unitless) and corrected biomass (CBM; $tonnes{\cdot}ha^{-1}$), coverage (number of 95% confidence intervals containing the true mean) and standard error correlations (*r*) by field PBA correction sample sizes for the western Newfoundland (NL) spacing trials

Factor	Field sample size[a]			
	5	10	15	20
$\%se\left(\overline{PBA}\right)$	7.08	7.08	7.03	7.07
$\%se\left(\overline{BBAR}\right)$	1.97	1.96	1.95	1.99
$\%se\left(\overline{FPBAR}\right)$	20.19	14.39	12.19	10.56
$\%se\left(\overline{CBM}\right)$	21.66	16.24	14.25	12.90
BM	157	156	155	155
Coverage	94.7	98.5	99.5	99.9
cor(PBA vs. FPBAR)	0.16	0.23	0.30	0.46
cor(PBA vs. BBAR)	0.00	0.05	0.04	0.08
cor(BBAR vs. FPBAR)	0.05	0.01	0.04	0.05

[a]Number of field sample points used to correct PBA.

error formulation. Bruce's method relies on independence of the component errors (Goodman, 1960). As shown in Figure 3, correlations (*r*) between the error components were quite low. The highest correlation was $r = 0.16$ ($r^2 = 0.03$) for $\%\mathbf{se}(\overline{\mathbf{PBA}})$ versus $\%\mathbf{se}(\overline{\mathbf{FPBAR}})$, while the other two correlations were less than 0.10 (Figure 4). We expanded our number of simulations to 1000 and assessed coverage (number of 95 per cent confidence intervals containing the true mean, as determined by the PSP measurements) by field sample size. For 5 field BA samples, coverage was 93.7 per cent, for 10 field BA samples, 98.6 per cent, for 15 field BA samples, 99.5 per cent and for 20 field BA samples, 99.9 per cent (Table 2).

Discussion

While selection of measure-trees did not produce biases, the underestimation of basal area from the spherical images (PBA) resulted in serious underestimation of biomass (Table 1, Figure 3). Occlusion issues with panoramic photo sampling were identified in several previous studies (Fastie, 2010; Dick, 2012; Lu *et al.,* 2019). In the field, occluded trees can be identified and correctly counted using a number of techniques including moving from plot centre to actually measuring distances and DBHs to determine if trees are in or out of the count sample (Kershaw *et al.,* 2016, pp. 372–374). With panoramic or spherical images, it is not possible to move around and only visible trees can be counted and/or measured. Our use of a third-stage subsample to collect field plots to correct for occluded trees was an effective and efficient sampling procedure to correct PBA to account for occluded trees (Figure 3; Table 1). Based on the resulting correction ratios for field: photo BA (FPBAR, Table 4), about 70 per cent of the 'in' trees were identified on the spherical images. This is consistent with the results from Dick (2012) who reported 60–90 per cent of trees correctly counted depending on the BAF used and stand density. In this study, we used 3 image acquisition points offset from plot centre and averaged across the three photo samples. Wang (2019) found that this to be an effective strategy for reducing occlusion bias but that was not the case here, even though some of the spherical images were in common.

As few as 5 field counts were sufficient to correct the underestimation; however, the resulting standard errors were quite large (Table 1). The percent standard errors associated with FPBAR were, in general, quite large relative to the percent standard errors for the other components (PBA and BBAR versus FPBAR; Table 2). At 10 field samples, the resulting standard errors were comparable to the standard errors obtained using model assisted approaches (Dai 2021). With 20 subsamples, the standard errors were only about double the full field sample data. The full field samples required over 4000 trees be measured for DBH and HT, our procedure only required about 60 trees be measured.

Subsampling with ratio estimation is, in general, a very efficient method for correcting bias, reducing sample sizes and focusing sampling efforts on the level where variation is greatest (Iles, 2003, pp. 557; Yang *et al.,* 2019; Hsu *et al.,* 2020). In this study, we used simple random selection of field subsamples. Yang *et al.* (2019) showed that simple random sampling was as efficient and, in some cases, can be more efficient than variable probability selection methods for LiDAR assisted ratio estimation when sample sizes were small. Hsu *et al.* (2020) and Yang *et al.* (2019) showed that list sampling was the most effective variable probability selection approach for ratio estimation. List sampling requires prior knowledge of the covariate for all sample units (Kershaw *et al.,* 2016, pp. 353–356). Both Hsu *et al.* (2020) and Yang *et al.* (2019) showed that the sampling with probability proportional to prediction (3P) could also be effectively used. Hsu (2019) developed methods for implementing 3P sampling using spherical images. A variable probability approach most likely would improve the results presented here.

Comparing our estimated standard serrors for single replicated simulated samples to the standard deviations of the means across all samples, our extension of Bruce's formula to three dimensions appears reasonable. Coverage, based on 95 per cent confidence intervals, seem to also support this extension. Bruce's formula relies on the independence of errors among the hierarchical components of the sample (Goodman, 1960). As

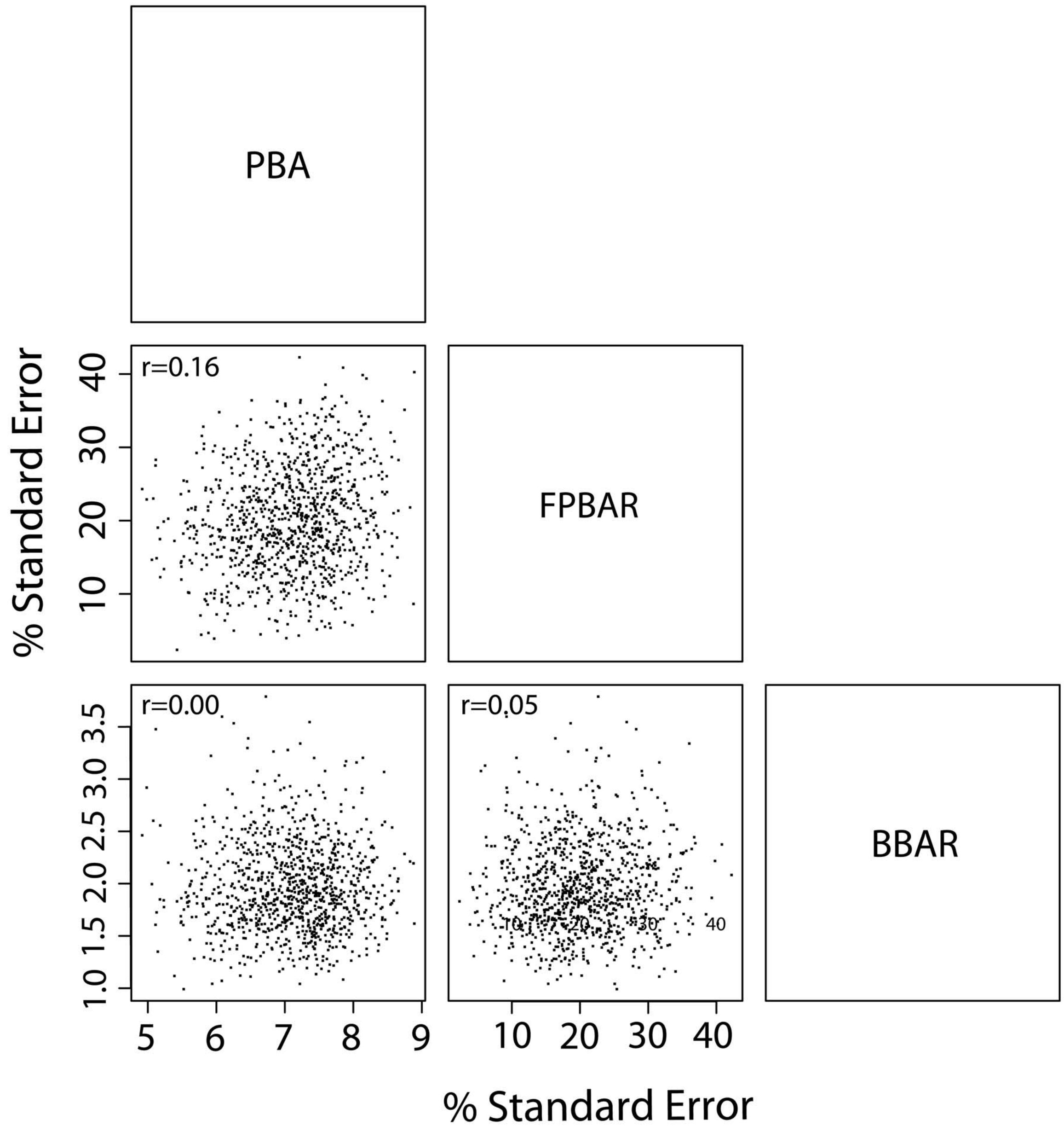

Figure 4 Pairwise comparisons and correlations (*r*) between standard errors for PBAs, field:photo basal area ratios (FPBAR) and biomass:basal area ratios (BBAR) for the Newfoundland (NL) spacing trials.

shown in Figure 3, the assumptions of independence appear to be met in this case, consistent with the observations of Gove *et al.* (2020) and Lynch *et al.* (2021, in press) that Bruce's formula provides adequate confidence interval coverage in simulations for ordinary big BAF sampling.

Conclusion

To make appropriate management decisions, foresters require accurate and timely data (Kershaw *et al.,* 2016, p. 3). An efficient sample design can not only reduce costs and save time but also provide accurate estimates (Lynch, 2017; Yang *et al.,* 2017; Chen *et al.,* 2019). In this study, we applied an alternative subsampling procedure using sectors to select measure-trees and coupled this with a hierarchal sampling scheme that combines spherical image measurements with horizontal point sample counts to estimate biomass in three spacing trials in western Newfoundland Island. Our results show that this approach is efficient and accurate and can be used to estimate biomass at a much lower cost than more expensive technology such as terrestrial LiDAR.

Data availability statement

Plot-level biomass estimates and photo-sector data used in this study are available at Dai and Kershaw (2021).

Acknowledgements

We are grateful to the Newfoundland and Labrador Department of Fisheries, Forestry and Agriculture for the use of their spacing trial data and allowing us access to acquire images on their study sites. The corresponding author is grateful for an Accelerated Master's Award from the New Brunswick Department of Postsecondary Education and Labour. We want to thank Dr Mike Lavigne, Mr Rodney Foster, Ms Greta Goodine of the Canadian Forest Service and Mr Cyril Lundrigan and Boyd Pittman of the Newfoundland and Labrador Department of Fisheries, Forestry and Agriculture for their assistance in data sharing, site location and project advice.

Conflict of interest statement

None declared.

Funding

Contribution Agreement with the Government of Newfoundland and Labrador; Natural Sciences and Engineering Research Council of Canada, Discovery Grant Program (RGPIN04280); New Brunswick Innovation Foundation Research Assistantship Initiative (RAI2017–032).

References

Armstrong, R.A. 1993 Remote sensing of submerged vegetation canopies for biomass estimation. *Int. J. Remote Sens.* **14**, 621–627.

Astrup, R., Ducey, M.J., Granhus, A., Ritter, T. and von Lüpke, N. 2014 Approaches for estimating stand-level volume using terrestrial laser scanning in a single-scan mode. *Can. J. For. Res.* **44**, 666–676.

Ayrey, E., Hayes, D.J., Fraver, S., Kershaw, J.A. and Weiskittel, A.R. 2019 Ecologically-based metrics for assessing structure in developing area-based, enhanced Forest inventories from LiDAR. *Can. J. Remote Sens.* **45**, 88–112.

Bartuska, A. 2006 *Why Biomass Is Important: The Role of the USDA Forest Service in Managing and using Biomass for Energy and Other Uses*. Research & Development, USDA Forest Service, pp. 1–16.

Baskerville, G. 1972 Use of logarithmic regression in the estimation of plant biomass. *Can. J. For. Res.* **2**, 49–53.

Bitterlich, W. 1984 *The Relascope Idea. Relative Measurements in Forestry*. Commonwealth Agricultural Bureaux.

Brown, S. 1997 *Estimating Biomass and Biomass Change of Tropical Forests: A Primer*. Food & Agriculture Org.

Brown, S. 1999 *Guidelines for Inventorying and Monitoring Carbon Offsets in Forest-Based Projects*. Winrock Int. World Bank Arlingt.

Brown, S. 2002 Measuring, monitoring, and verification of carbon benefits for forest–based projects Swingland, I.R., E.C. Bettelheim, J. Grace, G.T. Prance, and L.S. Saunders (eds.). *Philos. Trans. R. Soc. Lond. Ser. Math. Phys. Eng. Sci.* **360**, 1669–1683.

Brown, S., Gillespie, A.J. and Lugo, A.E. 1989 Biomass estimation methods for tropical forests with applications to forest inventory data. *For. Sci.* **35**, 881–902.

Chen, Y., Yang, T.-R., Hsu, Y.-H., Kershaw, J.A. and Prest, D. 2019 Application of big BAF sampling for estimating carbon on small woodlots. *For. Ecosyst.* **6**, 13.

Clark, J. and Murphy, G. 2011 Estimating forest biomass components with hemispherical photography for Douglas-fir stands in Northwest Oregon. *Can. J. For. Res.* **41**, 1060–1074.

Cleveland, W.S. 1981 LOWESS: a program for smoothing scatterplots by robust locally weighted regression. *Am. Stat.* **35**, 54.

Dai, X. 2021 *Novel methods for estimating above ground biomass. MScF Thesis*. University of New Brunswick.

Dai, X. and Kershaw, J. A. 2021. *Biomass Data from Sector Subsampling of 360° Spherical Images*. https://dataverse.lib.unb.ca/dataset.xhtml?persistentId=doi:10.25545/VCVEH1 (accessed on 8 April, 2021).

Dai, X., Wang, H., Ducey, M.J. and Kershaw, J.A. Jr. 2021. Sector subsampling for basal area ratio estimation: an alternative to big BAF sampling. *Can. J. For. Res.* (in press).

Dassot, M., Constant, T. and Fournier, M. 2011 The use of terrestrial LiDAR technology in forest science: application fields, benefits and challenges. *Ann. For. Sci.* **68**, 959–974.

DeCourt, N. 1956 *Utilisation de la photographie pour mesurer les surfaces terrières (The use of photography for measuring basal area). Rev. For. Fr. 8(7):505–507*. 7th edn. Rev. For. Fr, pp. 505–507.

Dick, A.R. 2012. *Forest inventory using a camera: concept, field implementation and instrument development MScF Thesis*. University of New Brunswick.

Dick, A.R., Kershaw, J.A. and MacLean, D.A. 2010 Spatial tree mapping using photography. *North. J. Appl. For.* **27**, 68–74.

Donnelly, J.G., Lavigne, M.B. and van Nostrand, R.S. 1986 *Precommercial Thinning Spacing Trials Established Between 1979 and 1985*. Newfoundland Forestry Centre.

Dubayah, R.O. and Drake, J.B. 2000 Lidar remote sensing for forestry. *J. For.* **98**, 44–46.

Ducey, M.J. and Astrup, R. 2013 Adjusting for nondetection in forest inventories derived from terrestrial laser scanning. *Can. J. Remote Sens.* **39**, 410–425.

Erfanifard, Y., Stereńczak, K., Kraszewski, B. and Kamińska, A. 2018 Development of a robust canopy height model derived from ALS point clouds for predicting individual crown attributes at the species level. *Int. J. Remote Sens.* **39**, 9206–9227.

Fassnacht, F.E., Hartig, F., Latifi, H., Berger, C., Hernández, J., Corvalán, P. *et al.* 2014 Importance of sample size, data type and prediction method for remote sensing-based estimations of aboveground forest biomass. *Remote Sens. Environ.* **154**, 102–114.

Fastie, C.L. 2010 Estimating stand basal area from forest panoramas. *Proc. Fine Int. Conf. Gigapixel Imaging Sci.* Carnegie Mellon University, Pittsburg, PA. 8p.

Gaveau, D.L. and Hill, R.A. 2003 Quantifying canopy height underestimation by laser pulse penetration in small-footprint airborne laser scanning data. *Can. J. Remote Sens.* **29**, 650–657.

Gleason, C.J. and Im, J. 2011 A review of remote sensing of forest biomass and biofuel: options for small-area applications. *GIScience Remote Sens.* **48**, 141–170.

Goetz, S.J., Baccini, A., Laporte, N.T., Johns, T., Walker, W., Kellndorfer, J. *et al.* 2009 Mapping and monitoring carbon stocks with satellite observations: a comparison of methods. *Carbon Balance Manag.* **4**, 2.

Goodman, L.A. 1960 On the exact variance of products. *J. Am. Stat. Assoc.* **55**, 708–713.

Gove, J.H., Gregoire, T.G., Ducey, M.J. and Lynch, T.B. 2020 A note on the estimation of variance for big BAF sampling. *For. Ecosyst.* **7**, 62.

Greaves, H.E., Vierling, L.A., Eitel, J.U.H., Boelman, N.T., Magney, T.S., Prager, C.M. *et al.* 2017 Applying terrestrial lidar for evaluation and calibration of airborne lidar-derived shrub biomass estimates in Arctic tundra. *Remote Sens. Lett.* **8**, 175–184.

Hayashi, R., Kershaw, J.A. and Weiskittel, A. 2015 Evaluation of alternative methods for using LiDAR to predict aboveground biomass in mixed species and structurally complex forests in northeastern North America. *MCFNS*. **7**, 49–65.

Hilker, T., van Leeuwen, M., Coops, N.C., Wulder, M.A., Newnham, G.J., Jupp, D.L.B. *et al.* 2010 Comparing canopy metrics derived from terrestrial and airborne laser scanning in a Douglas-fir dominated forest stand. *Trees*. **24**, 819–832.

Hopkinson, C., Lovell, J., Chasmer, L., Jupp, D., Kljun, N. and van Gorsel, E. 2013 Integrating terrestrial and airborne lidar to calibrate a 3D canopy model of effective leaf area index. *Remote Sens. Environ.* **136**, 301–314.

Hsu, Y.-H. 2019. *Applications of variable probability sampling using remotely sensed covariates. MSc Forestry Thesis*, University of New Brunswick. https://unbscholar.lib.unb.ca/islandora/object/unbscholar%3A9861.

Hsu, Y.-H., Chen, Y., Yang, T.-R., Kershaw, J.A. and Ducey, M.J. 2020 Sample strategies for bias correction of regional LiDAR-assisted forest inventory estimates on small woodlots. *Ann. For. Sci.* **77**, 1–12.

Iles, K. 2003 *A sampler of inventory topics*. Kim Isles & Associates Ltd.

Iles, K. and Smith, A.N. 2006 New type of sample plot that is particularly useful for sampling small clusters of objects. *For. Sci.* **52**, 148–154.

Kershaw, J.A., Ducey, M.J., Beers, T.W. and Husch, B. 2016 *Forest mensuration*. 5th edn. John Wiley & Sons.

Lambert, M.-C., Ung, C.-H. and Raulier, F. 2005 Canadian national tree aboveground biomass equations. *Can. J. For. Res.* **35**, 1996–2018.

Le Toan, T., Quegan, S., Davidson, M.W.J., Balzter, H., Paillou, P., Papathanassiou, K. *et al.* 2011 The BIOMASS mission: Mapping global forest biomass to better understand the terrestrial carbon cycle. *Remote Sens. Environ.* **115**, 2850–2860.

Lu, D. 2006 The potential and challenge of remote sensing-based biomass estimation. *Int. J. Remote Sens.* **27**, 1297–1328.

Lu, D., Chen, Q., Wang, G., Liu, L., Li, G. and Moran, E. 2016 A survey of remote sensing-based aboveground biomass estimation methods in forest ecosystems. *Int. J. Digit. Earth.* **9**, 63–105.

Lu, M.-K., Lam, T.Y., Perng, B.-H. and Lin, H.-T. 2019 Close-range photogrammetry with spherical panoramas for mapping spatial location and measuring diameters of trees under forest canopies. *Can. J. For. Res.* **49**, 865–874.

Lynch, T.B. 2017 Optimal plot size or point sample factor for a fixed total cost using the Fairfield Smith relation of plot size to variance. *Forestry* **90**, 211–218.

Lynch, T.B., Gove, J.H., Gregoire, T.G. and Ducey, M.J. 2021. An approximate point-based alternative for the estimation of variance under big BAF sampling. *For. Ecosyst.* (in press).

MacLean, R.G., Ducey, M.J. and Hoover, C.M. 2014 A comparison of carbon stock estimates and projections for the northeastern United States. *For. Sci.* **60**, 206–213.

Marshall, D.D., Iles, K. and Bell, J.F. 2004 Using a large-angle gauge to select trees for measurement in variable plot sampling. *Can. J. For. Res.* **34**, 840–845.

Mette, T., Papathanassiou, K. P., Hajnsek, I. and Zimmermann, R. 2002. Forest biomass estimation using polarimetric SAR interferometry. In *IEEE International Geoscience and Remote Sensing Symposium*. IEEE, pp. 817–819. http://ieeexplore.ieee.org/document/1025695/ (accessed on 11 May, 2020).

Montès, N., Gauquelin, T., Badri, W., Bertaudière, V. and Zaoui, E.H. 2000 A non-destructive method for estimating above-ground forest biomass in threatened woodlands. *For. Ecol. Manage.* **130**, 37–46.

Pearson, T. R. H., Brown, S. L. and Birdsey, R. A. 2007. *Measurement guidelines for the sequestration of forest carbon*. U.S. Department of Agriculture, Forest Service, Northern Research Station. https://www.fs.usda.gov/treesearch/pubs/13292 (accessed on 16 January, 2020).

Perng, B.-H., Lam, T.Y. and Lu, M.-K. 2018 Stereoscopic imaging with spherical panoramas for measuring tree distance and diameter under forest canopies. *For. Int. J. For. Res.* **91**, 662–673.

R Development Core Team. 2019. *R: A Language and Environment for Statistical Computing*. The R Foundation for Statistical Computing, c/o Institute for Statistics and Mathematics. https://www.r-project.org/.

Räsänen, A., Kuitunen, M., Tomppo, E. and Lensu, A. 2014 Coupling high-resolution satellite imagery with ALS-based canopy height model and digital elevation model in object-based boreal forest habitat type classification. *ISPRS J. Photogramm. Remote Sens.* **94**, 169–182.

Ricoh Imaging Company, LTD. 2016. *Rioch Theta S 360 video camera*. http://www.ricoh-imaging.co.jp/english/products/theta_s/ (accessed on 29 November, 2018).

Sales, M.H., Souza, C.M., Kyriakidis, P.C., Roberts, D.A. and Vidal, E. 2007 Improving spatial distribution estimation of forest biomass with geostatistics: A case study for Rondônia, Brazil. *Ecol. Model.* **205**, 221–230.

Smith, N.J. and Iles, K. 2012 Sector sampling—synthesis and applications. *Forests* **3**, 114–126.

Smith, N.J., Iles, K. and Raynor, K. 2008 Investigation of some sector sampling statistical properties. *For. Sci.* **54**, 67–76.

Stewart, B., Cieszewski, C.J. and Zasada, M. 2004 Using a camera as an angle gauge in angle-count sampling. In *Second International Conference on Forest Measurements and Quantitative Methods and Management*. Warnell School of Forestry and Natural Resources, University of Georgia, pp. 375–380.

Telenius, B. and Verwijst, T. 1995 The influence of allometric variation, vertical biomass distribution and sampling procedure on biomass estimates in commercial short-rotation forests. *Bioresour. Technol.* **51**, 247–253.

Usoltsev, V.A. and Hoffmann, C.W. 1997 Combining harvest sample data with inventory data to estimate forest biomass. *Scand. J. For. Res.* **12**, 273–279.

Wang, H. 2019. *Estimating forest attributes from spherical images. MSc Forestry Thesis*, University of New Brunswick. https://unbscholar.lib.unb.ca/islandora/object/unbscholar%3A10158

Wang, H., Kershaw, J.A., Yang, T.-R., Hsu, Y.-H., Ma, X. and Chen, Y. 2020 An integrated system for estimating forest basal area from spherical images. *Math. Comput. For. Nat. Resour. Sci.* **12**, 1–15.

Wang, H., Yang, T.-R., Waldy, J. and Kershaw, J.A. Jr. 2021. Estimating individual tree heights and DBHs from spherical images. *Math. Comput. For. Nat. Resour. Sci.* **13**, 1–14.

White, J.C., Coops, N.C., Wulder, M.A., Vastaranta, M., Hilker, T. and Tompalski, P. 2016 Remote sensing technologies for enhancing forest inventories: a review. *Can. J. Remote Sens.* **42**, 619–641.

Wilkes, P., Jones, S.D., Suarez, L., Mellor, A., Woodgate, W., Soto-Berelov, M. *et al.* 2015 Mapping forest canopy height across large areas by upscaling ALS estimates with freely available satellite data. *Remote Sens. (Basel)* **7**, 12563–12587.

Yang, T.-R., Hsu, Y.-H., Kershaw, J.A., McGarrigle, E. and Kilham, D. 2017 Big BAF sampling in mixed species forest structures of northeastern North America: influence of count and measure BAF under cost constraints. *For. Int. J. For. Res.* **90**, 649–660.

Yang, T.-R., Kershaw, J.A., Weiskittel, A.R., Lam, T.Y. and McGarrigle, E. 2019 Influence of sample selection method and estimation technique on sample size requirements for wall-to-wall estimation of volume using airborne LiDAR. *For. Int. J. For. Res.* **92**, 311–323.

Zar, J. 1999 Pearson Chi-square. In *Biostat. Anal. 4th Ed Up.* Saddle River NJ Prentice-Hall, pp. 25–30.

Zolkos, S., Goetz, S. and Dubayah, R. 2013 A meta-analysis of terrestrial aboveground biomass estimation using lidar remote sensing. *Remote Sens. Environ.* **128**, 289–298.